Forest Chemicals Review
www.forestchemicalsreview.com
ISSN: 1520-0191
September-October 2021 Page No. 1091-1118
Article History: Received: 22 July 2021 Revised: 16 August 2021 Accepted: 05 September 2021 Publication: 31 October 2021

A Low Cost and High Reliability Permanent Magnet Synchronous Motor Control Platform: Design of Speed Sensorless Servo Controller Based on MRAS

Tao Huang[1], Xiaoteng Tang[2*], Xinliang Wu[1]
[1]Modern Engineering Training Center, Xiamen University of Technology, Xiamen, Fujian, China
[2]Fujian Provincial Education Department Key Laboratory of Advanced Motion Control, Minjiang University, Fuzhou, Fujian, China
*Corresponding Author.

Abstract:

It's necessary for engineers and designers to get a low-cost and reliable permanent magnet synchronous motor control platform, so a permanent magnet synchronous motor sensorless servo control platform based on TI's low-cost DSP chip TMS320F2812 is designed in this paper. In the aspect of hardware, the design of various signal acquisition circuits and motor drive circuits are introduced in detail. At the same time, special attention is paid to the isolation of strong and weak current and the protection measures of intelligent power module. In the aspect of software, taking Model Reference Adaptive System approach as the core, the relationships and implementation methods of AD adoption, stator volotage calculation, CLARK Transform, estimation of flux linkage and torque, speed estimation are introduced. At the end of the paper, three experiments are carried out: PWM wave generation, position and speed estimation signal verification and system closed-loop. The experimental results verify that the designed control platform has strong control function, stable working performance, low cost because of abandoning speed/position sensor such as encoder. A wide application prospect can be expected.

***Keywords**: Low cost, High reliability, Permanent Magnet Synchronous Motor, Sensorless.*

I. INTRODUCTION

With the development of microcomputer technology, sensor technology and motor controltheory, the research and popularization of Permanent Magnet Synchronous Motor (PMSM) control system has received widespread attention[1-2]. PMSM has gradually become a commonly used servo motor in

Forest Chemicals Review
www.forestchemicalsreview.com
ISSN: 1520-0191
September-October 2021 Page No. 1091-1118
Article History: Received: 22 July 2021 Revised: 16 August 2021 Accepted: 05 September 2021 Publication: 31 October 2021

industrial control field due to its advantages of high precision, high reliability and wide speed regulation range[3-6]. In the high-performance control system of servo motor, high-precision rotor speed and position sensor is usually used as the feedback element of rotor speed and position signal. The use of the sensor increases the cost of the system and probability of failure. In order to overcome these problems caused by speed and position sensor, sensorless technology of servo motor drive has attracted great interest in recent years. Many sensorless control methods have been proposed in the literature of PMSM[7-23].

References [8] proposed a sensorless control technology of PMSM based on rotor flux orientation. The disadvantage of this method is that DC offset will lead to flux measurement error and affect rotor speed estimation. In addition, this method has good performance at rated speed, but it is not suitable for low-speed and zero speed operation.

Many researchers use the extended Kalman fifilter (EKF) technique to estimate the speed and the rotor position of the PMSM. Some authors use the dynamic model of the PMSM in d–q axis in the synchronous reference frame fifixed to the rotor[9-11] and others use the PMSM model in the $\alpha-\beta$ axis in the stationary reference frame fifixed to the stator [12]. It is well known that the method of EKF is not sensitive to unknown measurement noise. At the same time, there are multiple matrix operations in EKF algorithm, which still needs a long time to calculate these matrices. Accurary of the previous methods of estimating the rotor position of PMSM is affected by motor parameters. To overcome this problem, References [13,14] proposed a robust solution for rotor position estimation of PMSM based on sliding mode observer (SMO). SMO uses the estimated speed to update the estimated stator current in the sliding mode surface. Other methods are based on high carrier-frequency injection (CFI) technology where the signal is superimposed onto the fundamental phase voltages[15-18]. In most cases, the injected signal is a sinusoidal voltage. Therefore, this may lead to noise, motor current distortion, torque pulsation and large harmonic loss. The last techniques for sensorless PMSM are based on MRAS approach[19-23]. Instantaneous reactive power is used for rotor speed estimation in references[19, 20]. The advantage of this method is that the stator resistance is independent and less sensitive to the parameters of PMSM. But these observers mostly depend on motor parameters which vary with temperature. In order to overcome this problem, an on-line parameter identification method using adaptive algorithm is proposed in [21]. The author uses stator current for non-salient PMSM to estimate rotor speed and position based on MRAS adaptive strategy in [22-23].

In addition to the speed and position sensors, the economy of a permanent magnet motor servo control system also depends on its implementation method. In order to verify the accuracy of proposed algorithm some researchers using dSPACE to connect with PC[24-26], which can easily compile simulation software such as MATLAB and present the actual operation results of the algorithm designed

Forest Chemicals Review
www.forestchemicalsreview.com
ISSN: 1520-0191
September-October 2021 Page No. 1091-1118
Article History: Received: 22 July 2021 Revised: 16 August 2021 Accepted: 05 September 2021 Publication: 31 October 2021

in the simulation software in hardware, but the high price of dSPACE is difficult for most researchers to accept. Other researchers mentioned in their research results[27-29] that some DSP chips or other microprocessors were used to build the software and hardware platform in the verification process, but did not give the specific design and construction process, which has limited reference value for production and practitioners.

By comparing the methods proposed in the previous literature, we can note that MRAS technology is one of the best methods for estimating rotor speed and position due to its performance in term of requires less calculation time, to its easy implementation in DSP, and to its straight forward stability approach[11]. In addition, MRAS technology has been widely used in the joint estimation of stator resistance and rotor speed of PMSM. The most attractive element is that MRAS Speed estimator is simple in design. This is the most significant advantage of MRAS over other speed observers and is recommended for low-cost applications. Based on a low-cost DSP chip TMS320F2812 as the core, this paper introduces the design of hardware platform and software in detail. On the premise of fully considering the reliability and safety of the system, the current and voltage detection circuit and motor drive circuit are designed. At the same time, in order to evaluate the speed and rotor position estimation results of speed observer, a speed sensor detection circuit using high-precision photoelectric encoder will also be introduced in detail in this paper; In terms of software, the direct torque control technology is used as the framework, the speed sensorless technology adopts MRAS approach, and the pulse width modulation wave generated by SVPWM.

The organization structure of this paper is as follows: the second section introduces the hardware design process of PMSM controller, including control object, various detection circuits and driving circuits; The third section introduces the design process of PMSM controller DSP software, including the overall design process of the software, the design of program initialization and the design of underflow interrupt service program; The fourth section is the experimental verification of the designed control platform.

II. PMSM CONTROLLER HARDWARE DESIGN

2.1 Hardware Platform and Controlled Object

The hardware platform of PMSM DTC system mainly consists of driving circuit (including inverter circuit), signal detection circuit, central processing unit and experimental motor (control object). The overall block diagram of the hardware platform is shown in Fig 1.

Forest Chemicals Review
www.forestchemicalsreview.com
ISSN: 1520-0191
September-October 2021 Page No. 1091-1118
Article History: Received: 22 July 2021 Revised: 16 August 2021 Accepted: 05 September 2021 Publication: 31 October 2021

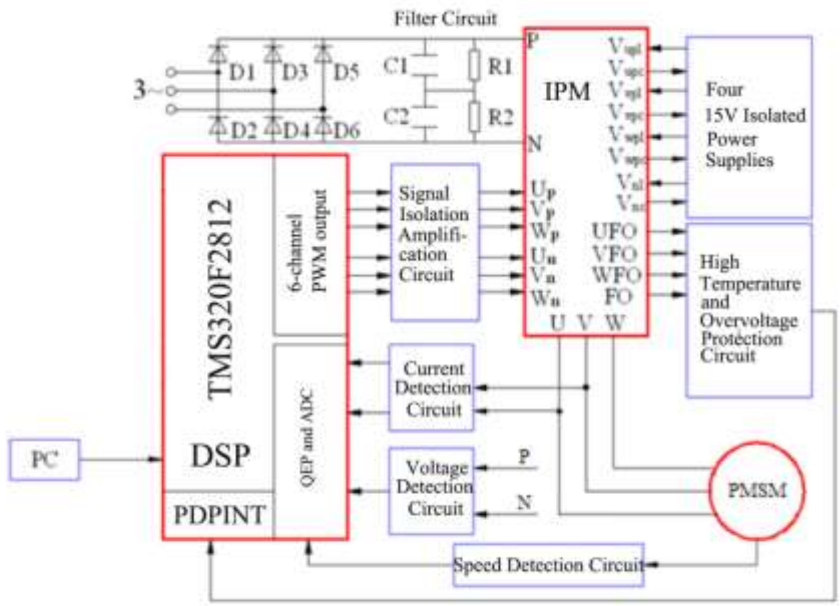

Fig 1: overall block diagram of hardware platform

Three-phase alternating current is input into intelligent power module (IPM) through three-phase rectifier circuit and filter circuit. The IPM is powered by four groups of isolated 15V power supplies (the isolation voltage needs to reach 1000V). At the same time, IPM can generate high-temperature and over voltage signals, which can be input into PDPINT port of DSP through conditioning circuit to protect IPM. Under the control of 6-channel PWM signals output by DSP, IPM generates three-phase electricity (A,B,C) transmitted to PMSM. The platform can collect A and B phase currents and bus voltage values and input them into DSP analog-to-digital converter (ADC) to form a feedback circuit. In order to facilitate the comparison with theestimated speed and position, the platform uses the encoder to measure the actual position and speed of the motor.

The servo controller is designed for the 600W AC permanent magnet synchronous servo motor produced by Fujian Mindong Yanan motor group, which is a surface mounted permanent magnet synchronous motor. The specific technical parameters are shown in TABLE I.

TABLE I. Technical parameters of motor

Rated torque (T_{eN})	Bus voltage (U_{dc})	Rated speed (ω_N)	Stator resistance (R_s)
3Nm	300V	3000rpm	3.6 Ω
Rated Power P_n	Rated current	Rotor flux linkage (Ψ_f)	Polar logarithm (p)
600W	2.5A	0.1827Wb	4
Moment of	Viscosity	Maximum output	Electrical time

Forest Chemicals Review
www.forestchemicalsreview.com
ISSN: 1520-0191
September-October 2021 Page No. 1091-1118
Article History: Received: 22 July 2021 Revised: 16 August 2021 Accepted: 05 September 2021 Publication: 31 October 2021

inertia (J)	coefficient (F)	torque (T_{Lm})	constant
$0.00031kg.m^2$	0.0003035N.m.s	6Nm	2.3ms
Self inductance of d-axis (L_d)	Self inductance of q-axis (L_d)		
8.23mH	8.23mH		

2.2 Signal Detection Circuit

Stator current and terminal voltage, which are necessary quantities for motor stator flux estimation in reference model adaptive algorithm, are collected by signal acquisition circuits, and their accuracy directly affects the performance of PMSM direct torque control system. TMS320F2812 internally integrates a 12-bit resolution analog-to-digital converter (ADC) with pipeline structure. There are 16 sampling channels in this chip, which are divided into two groups: ADCINAO~ADCINA7 and ADCINB0~ ADCINB7. It is considered that the three- phase current of the motor is balanced, Therefore, two current signals and one voltage signal can be collected into the ADC of DSP, and take ADCINA0, ADCINA1 and ADCINA2 as three AD channels to collect A phase current I_a, B phase current I_b and bus voltage U_{dc} respectively.

The QEP function of TMS320F2812 and CAP3 capture interrupt can be used to accurately measure the actual speed and position of the motor.

2.2.1 Current detection circuit

As shown in Fig 2, the current detection circuit uses LA55-P as the current sensor, produced by LEM, to detect the currents of phase A and phase B in real time. LA55-P is a high-precision current sensor, which can collect the maximum current of ±50A under ±15V power supply, the maximum output sample current is ±50mA, and the sampling error at room temperature is 0.9%, and the linear error is less than 0.15%.

Forest Chemicals Review
www.forestchemicalsreview.com
ISSN: 1520-0191
September-October 2021 Page No. 1091-1118
Article History: Received: 22 July 2021 Revised: 16 August 2021 Accepted: 05 September 2021 Publication: 31 October 2021

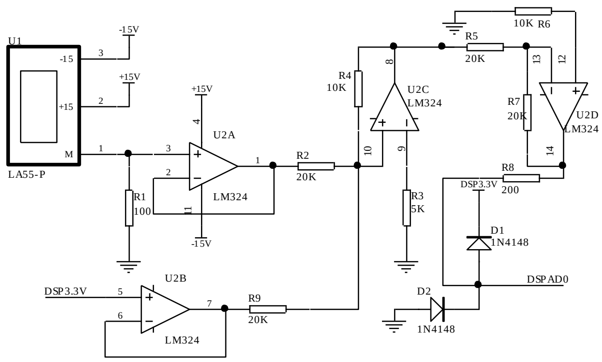

Fig 2: Current detection circuit

Assuming that the input current is I_iA and the output voltage is U_0V (the voltage input into DSP), analyze the circuit shown in Fig 2:

When the input current is 50A, the output current of LA55-P is 50mA, and the linearity of LA55-P is very good, so when the input current is I_i(-30~30)A, the output current of LA55-P is I_imA. As the rated current of the controlled object is 2.5A (as shown in TABLE I), the maximum absolute value of the stator current will not exceed 30A, and R_1 is set to 100Ω. As shown in Fig 2, the input voltage of the third pin of LM324 is (I_i/10) V. After passing through the voltage follower,The output voltage of pin 1 is still (I_i/10) V, and the output voltage of pin 7 is 3.3V. If LM324 is regarded as an ideal operational amplifier, pin 10 and pin 9 are virtual short, then the voltage of pin 10 (U_{10}) is 0V, and the analysis amplifier U2C can get the output U_8:

$$U_8 = \frac{33 + I_i}{20} V \tag{1}$$

Therefore, the input-output relationship as shown in formula (2) can be obtained:

$$U_0 = U_8 = \frac{33 + I_i}{20} V \tag{2}$$

Two zener diodes(1N4148) can keep the U_0 between 0 and 3.3V. Therefore, this circuit can adjust the input current of -30A-30A to the voltage of 0~ 3V and input this voltage to the ADC of DSP to ensure the normal operation of DSP chip.

2.2.2 Bus voltage detection circuit

The motor terminal voltage is obtained by reconstructing the DC bus voltage and the IGBT

Forest Chemicals Review
www.forestchemicalsreview.com
ISSN: 1520-0191
September-October 2021 Page No. 1091-1118
Article History: Received: 22 July 2021 Revised: 16 August 2021 Accepted: 05 September 2021 Publication: 31 October 2021

switching state in IPM. Therefore, if the IGBT switch state is known, only DC bus voltage is needed to obtain the motor terminal voltage.

LV25-P of LEM company is used to detect bus voltage. LV25-P can measure the voltage in the range of 10-500V under ±15V power supply. The maximum absolute value of input current cannot exceed 10mA. When the input current is 10mA, LV25-P outputs 25mA current. At room temperature, the sampling error is ±0.8%, and the linear error is less than 0.2%. The circuit is shown in Fig 3.

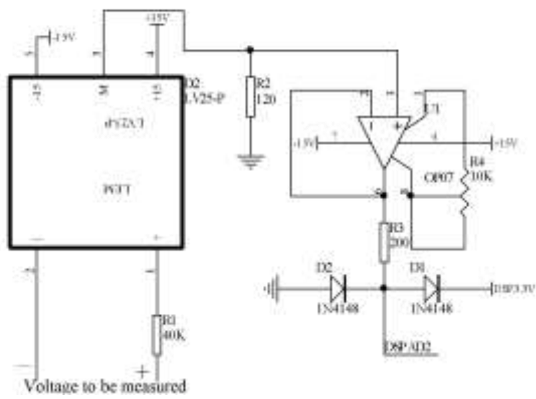

Fig 3: Bus voltage detection circuit

Selection of Rl: LV25-P is to measure the input voltage by measuring the input current. The rated bus voltage of PMSM controlled in this paper is 300V, so the maximum voltage measured by the sensor can be set as 400V, that is, when the input voltage is 400V, the input current of LV25-P is 10mA. Therefore, 40K/15W resistor is selected, but 5W resistor is difficult to obtain. Two 20K/12.5W resistors can be connected in series to form R1.

It can be seen from Fig 3 that the measured resistance is 120Ω, assuming that the amplifier OP07 is an ideal operational amplifier, at this time, if the input voltage is 400V, the LV25-P will output 25mA current. Since the input current of the ideal operational amplifier is almost zero, the input voltage of the third pin of OP07 is 3V, that is, the output voltage is 3V. According to the above analysis, it can be seen that the voltage to be measured from 0 to 400V should be linear corresponding to 0-3V at the ADC input of DSP, it not only ensures the correctness of voltage measurement, but also ensures the normal operation of DSP chip.

2.2.3 Encoder signal conditioning circuit for comparison

In order to obtain the actual motor speed conveniently, the photoelectric encoder, produced by Changchun Yuheng optics Co., Ltd., can be used to measure the speed and rotor position. It's a high

Forest Chemicals Review
www.forestchemicalsreview.com
ISSN: 1520-0191
September-October 2021 Page No. 1091-1118
Article History: Received: 22 July 2021 Revised: 16 August 2021 Accepted: 05 September 2021 Publication: 31 October 2021

precision encoder with 2500 yard wire/coil. This encoder have 15wires: A+, A-, B+, B-, Z+, Z-, U+, U-, V+, V-, W+, W-, +5V, 0V and a shielded wire. Phase A and phase B are two orthogonal differential pulse signals, and phase Z is a zero position differential pulse signal, U, V and W are three initial position differential pulse signals with phase difference of 120° respectively.

Since the power supply of encoder should be 5V, and its pulse output is also 5V, its signal can not be directly input into DSP for signal processing. So a signal conditioning circuit is needed to make the output pulse signals can be input into DSP and recognized by DSP chip. At the same time, it is noted that the attributes of these six signals are the same, so their conditioning circuits are the same, the following is an example of A-phase signal conditioning circuit. The schematic diagram of the signal conditioning circuit is shown in Fig 4.

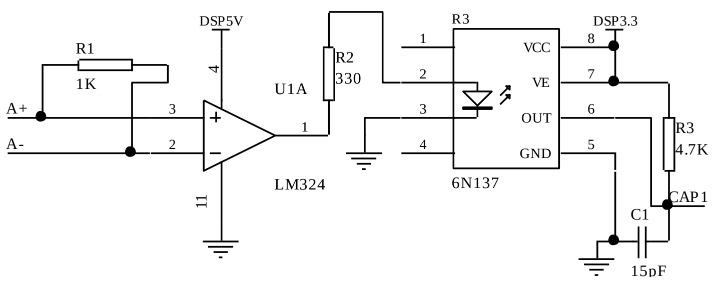

Fig 4: Circuit of encoder signal conditioning

The modulated signal of A phase is input to DSP CAP1, B phase input CAP2, Z phase input CAP3.

2.3 Motor drive circuits

The driving circuit adopts AC-DC-AC structure. In the inverter part, IPM is used, which integrates the driving circuit, the protection circuit and the power switch.

After comprehensively considering the performance, price and the matching of various parameters, the PM50RLA60 of Mitsubishi company is selected as the IPM for the platform. The maximum passing current of the IPM is 50A and the withstand voltage is 600V. The parameters of the IPM can refer to the data manual[30]. The internal structure of PM50RLA60 is shown in Fig 5.

The above-mentioned four groups of 15V power supply with 1000V+ isolation voltage can be supplied by Mitsubishi M57140-01, and its input voltage is 20VDC, which can output four groups of ±15V voltage with 1000V+ isolated voltage, meets the requirements of IPM power supply. The circuit is shown in Fig 6.

Forest Chemicals Review
www.forestchemicalsreview.com
ISSN: 1520-0191
September-October 2021 Page No. 1091-1118
Article History: Received: 22 July 2021 Revised: 16 August 2021 Accepted: 05 September 2021 Publication: 31 October 2021

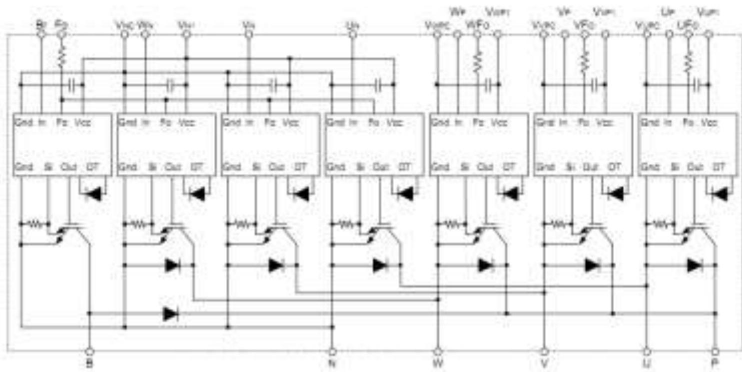

Fig 5: Internal structure diagram of PM50RLA60

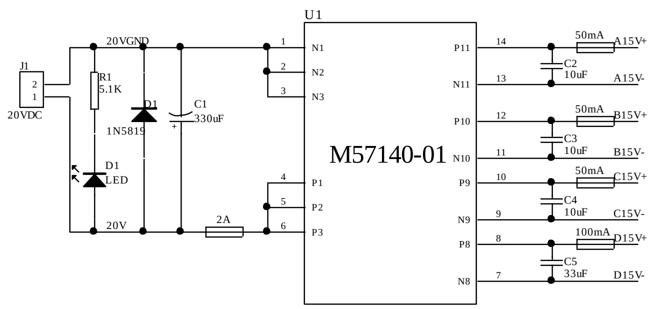

Fig 6: Drive power circuit of IPM

The PWM signal received by IPM generally adopts optocoupler driving circuit. The input of driving circuit is isolated from the control circuit by optocoupler, and an optocoupler with ideal switching speed is needed to avoid the influence on the driving performance. At the same time, in order to ensure that after passing through the optocoupler driving circuit, the isolation voltage of four groups of voltage for IPM is still kept 1000V+. It is recommended that HCP14504, produced by Agilent, be used. The isolation voltage is 1500V and the switching speed is less than 0.5μs; Taking PWM1 as an example, the driving circuit is shown in Fig 7.

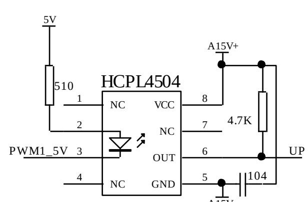

Fig 7: Optocoupler driving circuit

As shown in Fig 7 , the input voltage of the optocoupler driving circuit is 5V, and a certain driving current is required, which is not achieved by the PWM signal output of TMS320F2812, so in order to ensure the normal operation of IPM, 6N137 and 74HC245 are needed to form a signal isolation and

Forest Chemicals Review
www.forestchemicalsreview.com
ISSN: 1520-0191
September-October 2021 Page No. 1091-1118
Article History: Received: 22 July 2021 Revised: 16 August 2021 Accepted: 05 September 2021 Publication: 31 October 2021

amplification circuit to isolate and amplify signals, its circuit is shown in Fig 8.

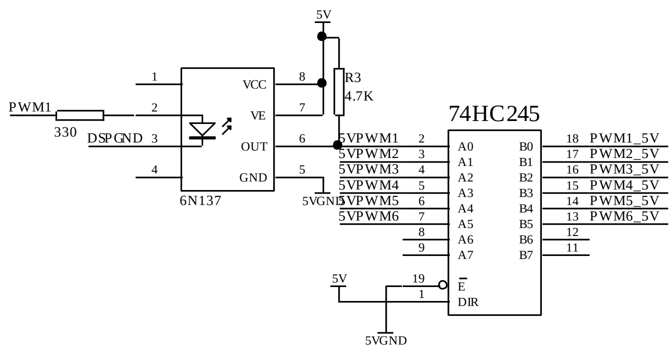

Fig 8: PWM signal isolation amplification circuit

IPM has the function of high temperature and over-voltage protection. When the temperature of IPM is too high or over-voltage occurs, a fault signal will be generated to "notify" the DSP chip's PDPINTA interface to make the output port in high resistance state to achieve the purpose of protecting IPM. The common optocoupler PC817 can be used to transmit the fault signal, which has 4 channels in total, the fault signals generated by them pass through monostable multivibrator 74HC21 and inverter 74HC04, and then input to the PDPINTA port of DSP through optocoupler PC817. The circuit is shown in Fig 9. At the same time, it is considered that PWM1 and PWM2, PWM3 and PWM4, PWM5 and PWM6 may not be reversed in the test process, in order to prevent the over temperature of IPM caused by this situation too frequently, three fault signals (PWM signal fault) are added to the fault circuit of the drive circuit. The signal is input to the monostable multivibrator 74HC21 shown in Fig 9 after passing through Schmidt trigger 74HC32. As long as any one of the seven channels produces fault signal, DSP will start fault protection measures to protect IPM.

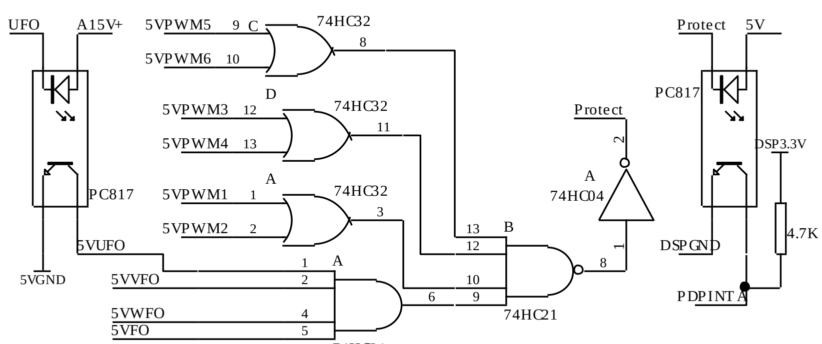

Fig 9: Fault signal transmission circuit

Forest Chemicals Review
www.forestchemicalsreview.com
ISSN: 1520-0191
September-October 2021 Page No. 1091-1118
Article History: Received: 22 July 2021 Revised: 16 August 2021 Accepted: 05 September 2021 Publication: 31 October 2021

III SOFTWARE DESIGN OF PMSM DIRECT TORQUE CONTROL SYSTEM

3.1 Overall Framework of PMSM Direct Torque Control System Software

The overall framework of PMSM direct torque control system software is shown in Fig 10.

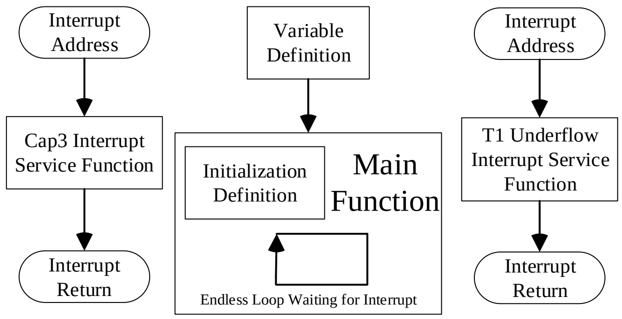

Fig 10: Overall software architecture diagram of PMSM direct torque control system

The software part of the system is mainly composed of variable definition, initialization program, main program and two interrupt programs. The main functions of the main program are initialize the system parameters, initialize the PIE interrupt controller, initialize the PIE interrupt vector table, call other initialization programs, open corresponding interrupts and wait for interrupts in an endless loop. The initialization program mainly includes PWM initialization, QEP initialization and ADC initialization. They mainly define the functions of each pin, enable various interrupts, and write corresponding control registers as needed. The two interrupt programs include T1 underflow interrupt and capture interrupt of capture 3(CAP3), complete the realization of PMSM sensorless direct torque control strategy and the function of motor position correction respectively. The initialization program and interrupt program are the core of the whole software system.

3.2 System Initialization Program

The definition of initialization program is directly related to the normal operation of the system, and it is an important design of PMSM direct torque control system software.

Analog-to-digital converter (ADC) initialization: ADCINA0, ADCINAl and ADCINA2 are defined as three AD sampling channels, and the ADC sampling is triggered by T1 underflow.

The main part of the direct torque control program is realized by T1 underflow interrupt service program, and ADC is also triggered by T1 underflow. In this way, the direct torque control program can make use of the voltage and current values in real time to make a series of calculations to generate appropriate IGBT switching time and compare with the value of T1 counter T1CNT (which can be

Forest Chemicals Review
www.forestchemicalsreview.com
ISSN: 1520-0191
September-October 2021 Page No. 1091-1118
Article History: Received: 22 July 2021 Revised: 16 August 2021 Accepted: 05 September 2021 Publication: 31 October 2021

regarded as the triangular carrier of SVPWM) to generate appropriate PWM wave, so that the PMSM speed can approach the reference speed. That is, twice the period register value (T1PR) of T1 represents the control period of the whole control system, the sampling period of ADC and the PWM period. The values of the period register T1PR and the control register T1CON can be defined as needed to complete the initialization of T1.

Define the dead time. The definition of the dead time needs to consider the switching time of IPM and the switching time of various optocouplers in the driving circuit, and then write the corresponding value into the dead time register DBTCONA (the system defines the dead time as 2μs). At the same time, it is necessary to define the values of PWM related registers to complete the setting of the following functions: space vector mode is prohibited, T1 counter is overloaded when underflow occurs, PWM1, 3 and 5 are active high, and PWM2, 4 and 6 are active low.

In order to cooperate with the orthogonal coding circuit for measuring the actual speed, an orthogonal coding circuit's capture interrupt initialization (QEP initialization) process is needed: the clock source of T2 is defined as QEP circuit, and its period register value is defined as four times of the number of code lines in one circle of encoder, and CAP1 and CAP2 are prohibited capture function, allow the capture function of CAP3. Further, in the process of implementation, the current actual speed of PMSM can be calculated by reading the values of two adjacent moments of T2CNT.

3.3 Interrupt Service Program

There are two interrupt service program in this system: T1 underflow interrupt service program and CAP3 interrupt service program. The CAP3 interrupt service program is used to correct the position of the motor. When the rotor of the motor turns to the 0 position (the encoderZ phase signal jumps), it enters the interrupt service program and updates the position variable to 0. The following focuses on the T1 underflow interrupt service program for PMSM sensorless direct torque control strategy.

Using the direct torque control strategy based on expected voltage described in reference [31](the control strategy block diagram is shown in Fig 11) and the PMSM speed estimation algorithm based on MRAS described in reference [32] (the speed estimation algorithm blockdiagram is shown in Fig 12), the T1 underflow interrupt service program is designed, and its flow chart is shown in Fig 13.

Forest Chemicals Review
www.forestchemicalsreview.com
ISSN: 1520-0191
September-October 2021 Page No. 1091-1118
Article History: Received: 22 July 2021 Revised: 16 August 2021 Accepted: 05 September 2021 Publication: 31 October 2021

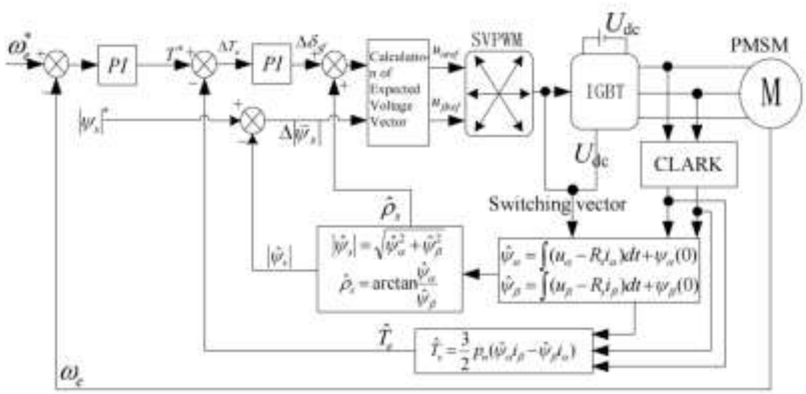

Fig 11: Block diagram of direct torque control strategy based on expected voltage

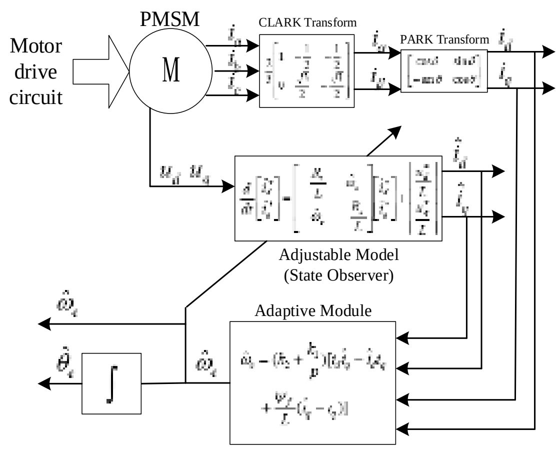

Fig 12: Block diagram of speed estimation algorithm based on MRAS

Forest Chemicals Review
www.forestchemicalsreview.com
ISSN: 1520-0191
September-October 2021 Page No. 1091-1118
Article History: Received: 22 July 2021 Revised: 16 August 2021 Accepted: 05 September 2021 Publication: 31 October 2021

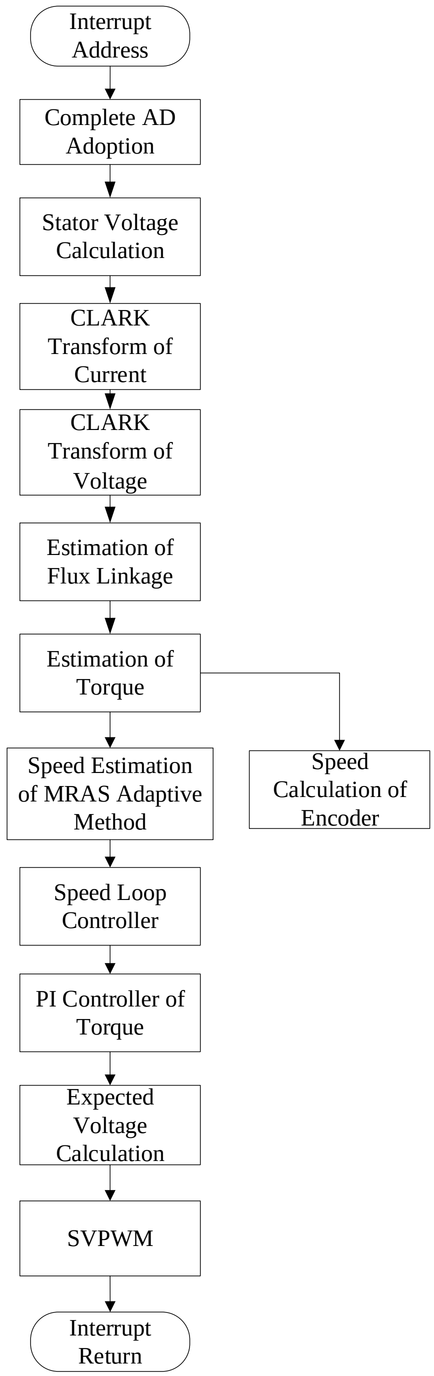

Fig 13: Flow chart of T1 underflow interrupt service program

In Fig 11-Fig 12, $\boldsymbol{\Psi}_s$ is stator flux vector, Ψ_α is flux linkage value of α-axis, u_α is stator voltage of α-axis , $u_{\alpha ref}$ is stator expected voltage of α-axis , R_s is stator resistance value, i_α is stator current of α-axis, Ψ_β is flux linkage of β-axis, u_β is stator voltage of β-axis , $u_{\beta ref}$ is stator expected voltage of

Forest Chemicals Review
www.forestchemicalsreview.com
ISSN: 1520-0191
September-October 2021 Page No. 1091-1118
Article History: Received: 22 July 2021 Revised: 16 August 2021 Accepted: 05 September 2021 Publication: 31 October 2021

β-axis, i_β is stator current of β-axis , p is the differential factor , p_n is the pole pairs of motor , i_d is stator current of d-axis, i_q is stator current of q-axis, u_d is stator voltage of d-axis, u_q is stator voltage of q-axis, ω_e is the electromagnetic speed of motor , θ_e is the electromagnetic position of motor rotor, T_e is output electromagnetic torque of motor, $\Delta\delta_{sf}$ is Torque angle increment, ρ_s is the spatial phase angle, L is the value of stator self inductance, Ψ_f is the value of rotor flux linkage. And $\square^*$ is the reference value of a variable, $\Delta\square$ is the difference between the actual or estimated value and the reference value, $\hat{\square}$ is the estimated value of a variable, $|\square|$ is the size of a vector.

The ADC module stores the sampling results of three AD channels, ADCINA0, ADCINAl and ADCINA2, in the result registers ADCRESULTO, ADCRESULT1 and ADCRESULT2 respectively. Each result register has 16 bits, while the ADC of TMS320F2812 has 12 bits, which are the upper 12 bits of the result register. Therefore, in the AD data processing program, it is necessary to shift the value of the result register to the right by 4 bits first. The following describes the data acquisition process by taking the data processing process of ADCINA0 as an example: 1) Run the AD conversion program when the input current is 0; 2) Read the ADCRESULT0 value at this time, and set this value as OFFSET0, which is the offset of phase A current; 3) Solve the AD conversion result according to formula (3).

$$I_a = \frac{I_{amax}(\mathrm{ADCRESULT0} \gg 4 - \mathrm{OFFSET0} \gg 4)}{4095} \tag{3}$$

Where I_{amax} is the maximum value of phase A current, and I_a is the measured value of phase A current.

According to Fig 11, the stator voltage is calculated from the switching value output by SVPWM module and the bus voltage obtained by AD sampling, and the stator current is obtained directly from AD sampling. They can get α-axis and β-axis components by CLARK transformation (refer to Fig 12 for CLARK transformation). According to the given formula in Fig 11, the estimated value of flux linkage is obtained, and then the estimated value of PMSM electromagnetic output torque is obtained. The estimated rotational speed and expected voltage vector are calculated by the specific algorithms of the PMSM rotational speed adaptive estimation module based on MRAS shown in Fig 12 and the expected voltage calculation module shown informula (4). In the process of software realization, the speed regulator is realized by PI regulator.

Forest Chemicals Review
www.forestchemicalsreview.com
ISSN: 1520-0191
September-October 2021 Page No. 1091-1118
Article History: Received: 22 July 2021 Revised: 16 August 2021 Accepted: 05 September 2021 Publication: 31 October 2021

$$\begin{cases} u_{\alpha ref} = R_s i_\alpha + \dfrac{|\bar{\psi}_s|\cos(\rho_s + \Delta\delta_{sf}) - |\bar{\psi}_s|\cos(\rho_s)}{T_s} \\ u_{\beta ref} = R_s i_\beta + \dfrac{(|\bar{\psi}_s| + \Delta|\bar{\psi}_s|)\sin(\rho_s + \Delta\delta_{sf}) - |\bar{\psi}_s|\sin(\rho_s)}{T_s} \end{cases} \tag{4}$$

The estimated value of flux linkage can be calculated by "flux estimation module" in Fig 11, but it includes an integral element. Based on the trapezoidal approximation principle , integral element in the flux estimation module can be realized by formula (5):

$$\hat{\Psi}_\alpha(k) = \hat{\Psi}_\alpha(k-1) + \frac{T_s}{2}[(u_\alpha - R_s i_\alpha)_k + (u_\alpha - R_s i_\alpha)_{k-1}] \tag{5}$$

Where $\hat{\Psi}_\alpha(k)$ is the flux estimation of the current control period, and $\hat{\Psi}_\alpha(k-1)$ is the estimated flux of last control period.

The encoder signal processing, PI regulator and SVPWM software implementation will be discussed in detail below.

3.3.1 Software Implementation of PI Regulator

In direct torque control system based on expected voltage vector, PI regulator is needed to adjust speed and torque. The system uses PI regulator with integral correction to adjust speed and torque, and PI regulator with integral correction can quickly desaturate. The algorithm blockdiagram is shown in Fig 14.

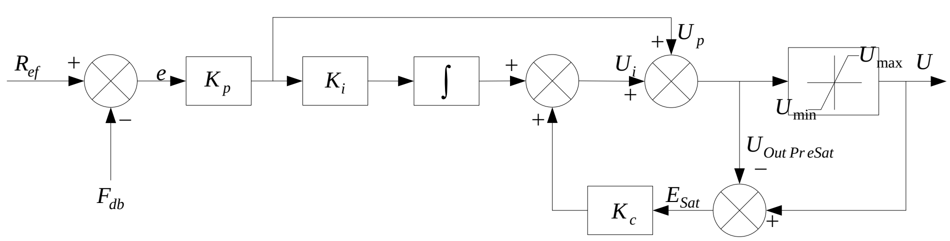

Fig 14: Algorithm block diagram of integral improved PI regulator

Forest Chemicals Review
www.forestchemicalsreview.com
ISSN: 1520-0191
September-October 2021 Page No. 1091-1118
Article History: Received: 22 July 2021 Revised: 16 August 2021 Accepted: 05 September 2021 Publication: 31 October 2021

The specific algorithm is shown in formula (6):

$$\begin{cases} U_p(k) = K_p e(k) \\ U_i(k) = U_i(k-1) + K_p K_i e(k) + K_c(U(k-1) - U_{Out\,PreSat}(k-1)) \\ U_{Out\,PreSat}(k) = U_p(k) + U_i(k) \end{cases} \tag{6}$$

where $U_p(k)$ is the output value of the proportional term, K_p is the proportional coefficient, $e(k)$ is the current error, K_i is the integral coefficient, K_c is the correction coefficient of the integral term, $U_i(k)$ is the output value of the integral term, and $U_{OutPreSat}$ is output value before limiting, U is the output, U_{max} and U_{min} are the maximum and minimum values of the output limiting pair respectively.

3.3.2 Software Implementation of SVPWM

The principle of SVPWM has been involved in many literatures. This paper only expounds the realization of SVPWM algorithm in DSP. According to the principle of SVPWM, in order to realize the real-time modulation of SVPWM signal, we should know the spatial phase of the expected voltage vector $\boldsymbol{U}_{\mathbf{ref}}$ and its sector firstly, and then synthesize the expected voltage vector by using two adjacent basic voltage vectors and appropriate zero vectors.

3.3.2.1 Determination of the sector where the expected voltage vector $\boldsymbol{U}_{\mathbf{ref}}$ is located

Expected voltage vector $\boldsymbol{U}_{\mathbf{ref}}$ is given by αβ coordinate system component form of u_α and u_β, each equivalent condition of the sector where $\boldsymbol{U}_{\mathbf{ref}}$ is located is shown in TABLE II According to TABLE II, the sector of expected voltage vector $\boldsymbol{U}_{\mathbf{ref}}$ is entirely up to u_β, $\sqrt{3}u_\alpha - u_\beta$ and $-\sqrt{3}u_\alpha - u_\beta$, three intermediate variable B_0, B_1, B_2 are defined by formula(7).

$$\begin{cases} B_0 = u_\beta \\ B_1 = \dfrac{\sqrt{3}}{2}u_\alpha - \dfrac{1}{2}u_\beta \\ B_2 = -\dfrac{\sqrt{3}}{2}u_\alpha - \dfrac{1}{2}u_\beta \end{cases} \tag{7}$$

TABLE II. Equivalent Condition of $\boldsymbol{U}_{\mathbf{ref}}$'s sector

The sector of $\boldsymbol{U}_{\mathbf{ref}}$	Equivalent Condition
I	$u_\alpha > 0,\ u_\beta > 0$ and $u_\beta/u_\alpha < \sqrt{3}$
II	$u_\alpha > 0$ and $u_\beta/\lvert u_\alpha\rvert > \sqrt{3}$
III	$u_\alpha < 0,\ u_\beta > 0$ and $-u_\beta/u_\alpha <$

Forest Chemicals Review
www.forestchemicalsreview.com
ISSN: 1520-0191
September-October 2021 Page No. 1091-1118
Article History: Received: 22 July 2021 Revised: 16 August 2021 Accepted: 05 September 2021 Publication: 31 October 2021

	$\sqrt{3}$
IV	$u_\alpha < 0,\ u_\beta < 0$ and $u_\beta/u_\alpha < \sqrt{3}$
V	$u_\beta < 0$ and $-u_\beta/\lvert u_\alpha\rvert > \sqrt{3}$
VI	$u_\alpha > 0,\ u_\beta < 0$ and $-u_\beta/u_\alpha < \sqrt{3}$

Redefinition: if B_0>0, then P_0=1, otherwise P_0=0; If B_1>0, then P_1=1, otherwise P_1=0; If B_2>0, then P_2=1, otherwise P_2=0. It is not difficult to see that there are 8 different combinations of P_0, P_1 and P_2, but because P_0, P_1 and P_2 are not 1 or 0 at the same time, the actual number of combinations is 6, the combinations of P_0, P_1 and P_2 have the relation of one-to-one correspondence with the sector of vector $\boldsymbol{U}_{\mathbf{ref}}$, let P=P_0,+2P_1+4P_2, look up TABLE III the sector of $\boldsymbol{U}_{\mathbf{ref}}$ can be obtained.

TABLE III Relationsip of the value of *P* and the sector

P	3	1	5	4	6	2
Sector	I	II	III	IV	V	VI

With this method, the sector of $\boldsymbol{U}_{\mathbf{ref}}$ can be determined only by simple addition, subtraction and logical operation. Compared with TABLE II, the response speed of the system can be improved.

3.3.2.2 Calculation of Action Time of Basic Voltage Vector

Assuming that $\boldsymbol{U}_{\mathbf{ref}}$ is in sector I, according to the analysis in reference [31], there are:

$$\begin{bmatrix} u_\alpha \\ u_\beta \end{bmatrix} T_{pwm} = \left|\vec{U}_{ref}\right| \begin{bmatrix} \cos\theta_u \\ \sin\theta_u \end{bmatrix} T_{pwm} = \frac{2}{3} U_{dc} \begin{bmatrix} 1 \\ 0 \end{bmatrix} T_1 + \frac{2}{3} U_{dc} \begin{bmatrix} \cos 60^\circ \\ \sin 60^\circ \end{bmatrix} T_2 \tag{8}$$

where θ_u is the spatial phase of $\boldsymbol{U}_{\mathbf{ref}}$, T_1 and T_2 are unknown, Solve this formulaand get formula (9).

Let $K = \sqrt{3}T_{\mathrm{pwm}}/U_{\mathrm{dc}}, X = u_\beta, Y = \sqrt{3}u_\alpha/2 + u_\beta/2, Z = -\sqrt{3}u_\alpha/2 + u_\beta/2$. Assuming that the first acting time of the basic voltage vector is T_x, and the second acting time is T_y. In the same way as the first sector calculation method, the relationship between the acting time of the basic voltage vector and X, Y and Z as shown in TABLE IV is obtained.

Forest Chemicals Review
www.forestchemicalsreview.com
ISSN: 1520-0191
September-October 2021 Page No. 1091-1118
Article History: Received: 22 July 2021 Revised: 16 August 2021 Accepted: 05 September 2021 Publication: 31 October 2021

$$\begin{cases} T_1 = \dfrac{\sqrt{3}T_{pwm}}{U_{dc}}(\dfrac{\sqrt{3}}{2}u_\alpha - \dfrac{u_\beta}{2}) \\ T_2 = \dfrac{\sqrt{3}T_{pwm}}{U_{dc}}u_\beta \\ T_0 = T_7 = \dfrac{T_{pwm} - T_1 - T_2}{2} \end{cases} \tag{9}$$

TABLE IV The relationship between the acting time of the basic voltage vector and X, Y and Z

Sector	I	II	III	IV	V	VI
T_x	-KZ	KZ	KX	-KX	-KY	KY
T_y	KX	KY	-KY	KZ	-KZ	-KX

Consider that when $T_x+T_y \geq T_{pwm}$, the endpoint of the vector exceeds the regular hexagonal boundary of the basic voltage vector, resulting in over modulation. If we continue to use the calculated T_x and T_y, the output waveform will be seriously distorted. So we can take the following measures to solve this problem:

$$\begin{cases} T_x' = T_x T_{pwm}/(T_x + T_y) \\ T_y' = T_y T_{pwm}/(T_x + T_y) \\ T_0 = T_7 = 0 \end{cases} \tag{10}$$

T_x' and T_y' calculated by formula (10) can replace the T_x and T_y above.

According to the above calculation, the acting time of the corresponding basic voltage vector and zero voltage vector can be obtained.

3.3.2.3 Calculation of DSP comparison register value

When the sector of expected voltage vector and the acting time of the corresponding basic voltage vector and zero vector are determined, the value of each corresponding comparison register can be calculated according to the PWM modulation principle. When the expected voltage vector is located in sector I, its operation relation is as follows[33]:

$$\begin{cases} t_{aon} = (T_{pwm} - T_x - T_y)/4 \\ t_{bon} = t_{aon} + T_x/2 \\ t_{con} = t_{bon} + T_y/2 \end{cases} \tag{11}$$

Forest Chemicals Review
www.forestchemicalsreview.com
ISSN: 1520-0191
September-October 2021 Page No. 1091-1118
Article History: Received: 22 July 2021 Revised: 16 August 2021 Accepted: 05 September 2021 Publication: 31 October 2021

where t_{aon}, t_{bon}, t_{con} are the values of the corresponding comparison registers respectively. The values of comparison registers corresponding to different sectors are shown in TABLE V.

Table V The correspondence between comparison register values and sectors

Sector	**I**	**II**	**III**	**IV**	**V**	**VI**
T_a	t_{aon}	t_{bon}	t_{con}	t_{con}	t_{bon}	t_{aon}
T_b	t_{bon}	t_{aon}	t_{aon}	t_{bon}	t_{con}	t_{con}
T_c	t_{con}	t_{con}	t_{bon}	t_{aon}	t_{aon}	t_{bon}

T_a, T_b and T_c are the values of the corresponding three-phase comparison registers. Writing T_a, T_b and $T_c$into the comparison registers CMPR1, CMPR2 and CMPR3 respectively, that is the whole algorithm of SVPWM completed.

IV EXPERIMENT AND RESULTS ANALYSIS

4.1 Experiment of generating PWM wave

Before using PWM wave to drive motor, it must be determined whether the PWM wave generated by SVPWM module is correct. The modulation wave function[33] of the phase voltage is shown in formulas (12) and (13).

$$U_{\mathrm{a}}(\theta_{\mathrm{u}}) = \begin{cases} \frac{\sqrt{3}}{2}|U_{\mathrm{ref}}|\cos(\theta_{\mathrm{u}} - \frac{\pi}{6}) & Sector\ 1,4 \\ \frac{\sqrt{3}}{2}|U_{\mathrm{ref}}|\cos(\theta_{\mathrm{u}}) & Sector\ 2,5 \\ \frac{\sqrt{3}}{2}|U_{\mathrm{ref}}|\cos(\theta_{\mathrm{u}} + \frac{\pi}{6}) & Sector\ 3,6 \end{cases} \tag{12}$$

$$\begin{cases} U_b(\theta_u) = U_a(\theta_u - \frac{2\pi}{3}) \\ U_c(\theta_u) = U_a(\theta_u - \frac{4\pi}{3}) \end{cases} \tag{13}$$

The modulated wave function[33] of line voltage is derived from formulas (12) and (13), as shown in formula (14).

Forest Chemicals Review
www.forestchemicalsreview.com
ISSN: 1520-0191
September-October 2021 Page No. 1091-1118
Article History: Received: 22 July 2021 Revised: 16 August 2021 Accepted: 05 September 2021 Publication: 31 October 2021

$$\begin{cases} U_{ab}(\theta_u) = \sqrt{3}\left|U_{ref}\right|\sin(\theta_u + \dfrac{2\pi}{3}) \\ U_{bc}(\theta_u) = U_{ab}(\theta_u - \dfrac{2\pi}{3}) \\ U_{ca}(\theta_u) = U_{ab}(\theta_u - \dfrac{4\pi}{3}) \end{cases} \tag{14}$$

From formulas (12) to (14), it can be seen that the phase voltage modulation wave function is saddle shaped, while the line voltage modulation wave function is sine shaped. In CCS, whether the waveform of T_a is saddle shape or not and whether the waveforms of T_a-T_b are sine shape can be observed to determine whether the PWM wave is correct or not.

Using software method, generate an expected voltage vector and make it rotate at a certain angular speed. Connect CCS with DSP main control board, run the program and draw, and get T_a and T_a-T_b waveforms, as shown in Fig 15 and Fig 16.

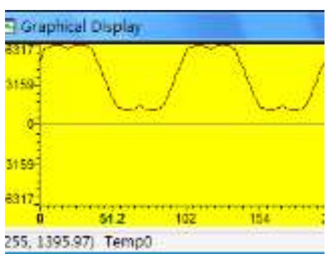

Fig 15: The wave of T_a

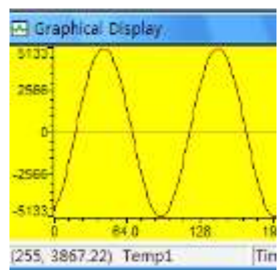

Fig 16: The wave of T_a-T_b

It can be seen from Fig 15 and Fig 16 that the SVPWM program can generate correct PWM wave, which indicates that the module is correctly written.

4.2 Verification Experiment of Position and Speed Estimation Signals

The experiment is mainly used to verify whether the motor position signal obtained by MRAS estimation algorithm is correct. Considering the safety and other reasons, the bus voltage is supplied with 12V DC power by voltage stabilizing source. During the test, a rotating voltage vector is input to the SVPWM module, if the phase of the voltage vector corresponds to the actual electromagnetic position of the motor rotor, the motor can be driven to start and finally rotate at a stable speed.

The rotation voltage vector is obtained by the given quadrature axis components U_d和U_q of the voltage vector, and the position signal required by IPARK is obtained θ calculated by MRAS module.

Forest Chemicals Review
www.forestchemicalsreview.com
ISSN: 1520-0191
September-October 2021 Page No. 1091-1118
Article History: Received: 22 July 2021 Revised: 16 August 2021 Accepted: 05 September 2021 Publication: 31 October 2021

Only when the position estimation signal $\hat{\theta}$ obtained by MRAS module is approximately equal to the actual electromagnetic position θ of the controlled motor rotor, the motor continue to rotate.

Set U_d=0, U_q=5, the program is runned in CSS, the following result can be obtrained:

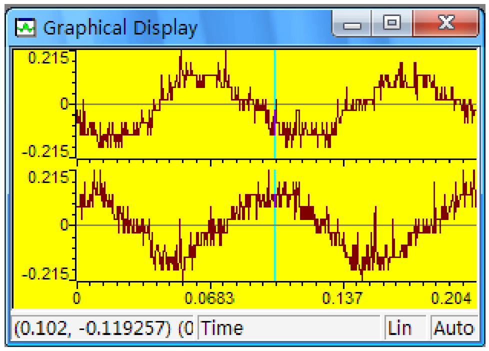

Fig 17: Phase A and phase B currents for U_q= 5

In Fig 17, phase a current is shown at the top and phase B current at the bottom.

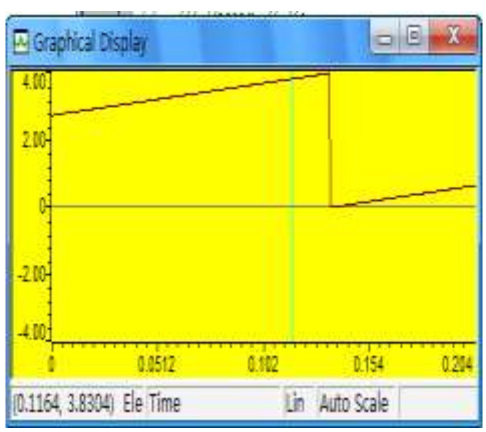

Fig 18: Estimated value of motor electromagnetic position for U_q=5

Forest Chemicals Review
www.forestchemicalsreview.com
ISSN: 1520-0191
September-October 2021 Page No. 1091-1118
Article History: Received: 22 July 2021 Revised: 16 August 2021 Accepted: 05 September 2021 Publication: 31 October 2021

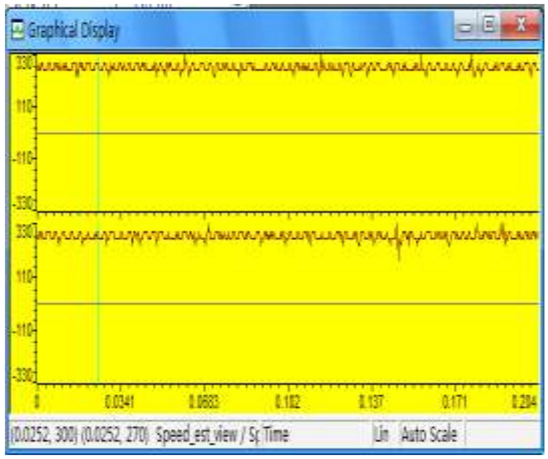

Fig 19: Comparsion of electromagnetic estimated speed and actual electromagnetic speed for U_q=5

Estimated value of motor electromagnetic position for U_q=5 is shown in Fig 18. And in Fig 19, the upper part shows the estimated electromagnetic speed and the lower part shows the actual electromagnetic speed.

From the analysis and results above, the MRAS program can accurately estimate the rotor position and speed of the motor, and can be used in the next double closed loop (speed closed-loop and flux closed-loop) experiment.

4.3 Experiment of Closed-loop

In order to ensure the safety during the experiment, the same 12V regulated power supply is connected, and different reference speeds are set to observe the stator current and speed curve.

Set the reference speed to 500rpm, run at no load, and get results as shown in Fig 20 and Fig 21. The reference speed is set at 300rpm, and a constant load is applied to the motor to obtain the result diagram shown in Fig 22. Slightly increase the load and get the result as shown in Fig 23. Add a time-varying load, run the program, and get the result as shown in Fig 24.

Forest Chemicals Review
www.forestchemicalsreview.com
ISSN: 1520-0191
September-October 2021 Page No. 1091-1118
Article History: Received: 22 July 2021 Revised: 16 August 2021 Accepted: 05 September 2021 Publication: 31 October 2021

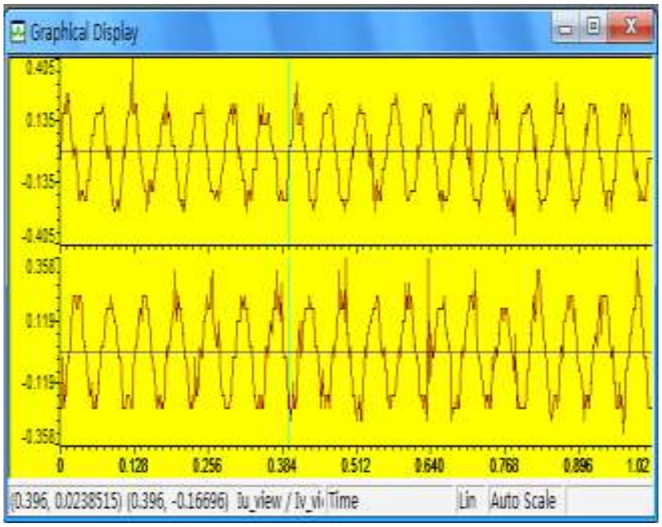

Fig 20: A phase and B phase currents for the reference speed is 500rpm

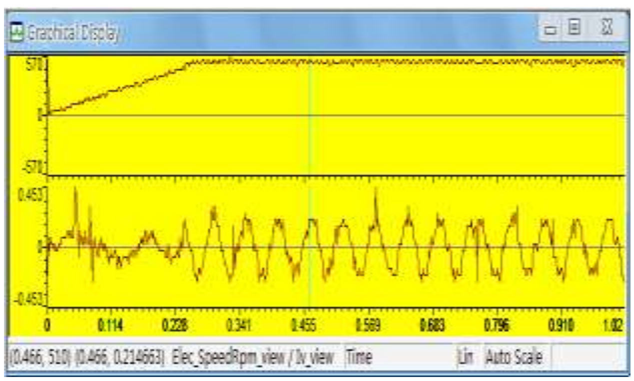

Fig 21: Electromagnetic speed and B phase current for the reference speed is 500rpm

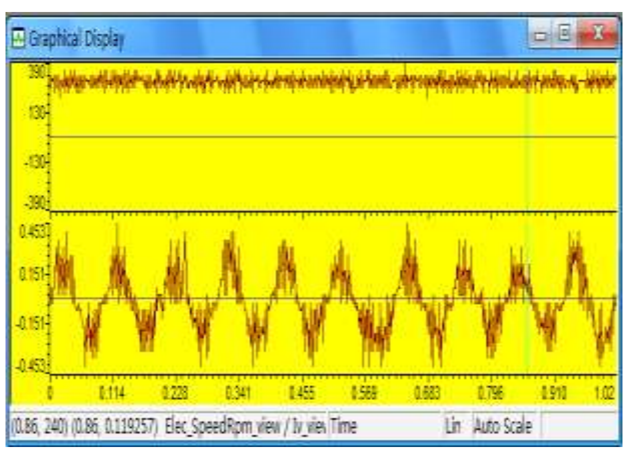

Fig 22: Electromagnetic speed and B phase current with reference speed of 300rpm and constant load

Forest Chemicals Review
www.forestchemicalsreview.com
ISSN: 1520-0191
September-October 2021 Page No. 1091-1118
Article History: Received: 22 July 2021 Revised: 16 August 2021 Accepted: 05 September 2021 Publication: 31 October 2021

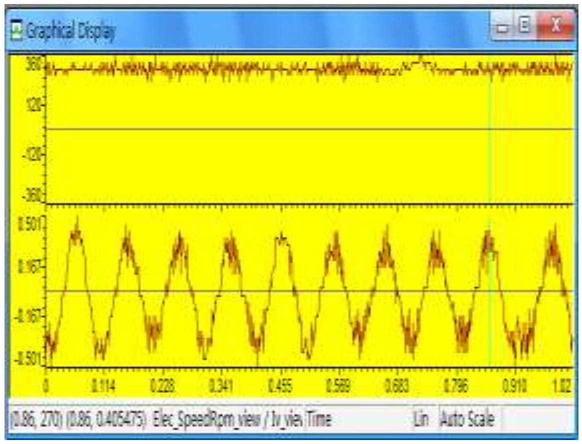

Fig 23: Electromagnetic speed and B phase current with slightly increased load

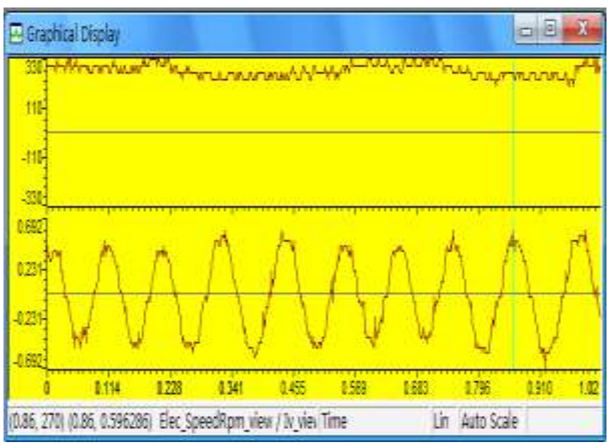

Fig 24: Electromagnetic speed and B phase current with time-varying load

From the above result chart, it can be seen that the system can better follow the given speed and achieve the purpose of speed regulation. At the same time, the system also has good speed regulation effect after adding load.

V. CONCLUSION

In this paper, a low-cost and reliable permanent magnet synchronous motor servo control platform is designed. In order to achieve the goal of low cost, the platform uses MRAS approach to estimate the motor rotor speed and position, and uses the cheap DSP chip TMS320F2812 as the control chip; In order to achieve the goal of high reliability, the strong and weak current isolation, high temperature and overvoltage protection are fully considered in the hardware design, and the IPM is used as the core of the driving circuit. According to the obtained results, we can have the following remarks:

(i) PWM wave generation experiment can get the correct phase voltage and line voltage modulation waveform, which proves that the SVPWM implementation approach proposed in this paper can generate the correct PWM wave.

(ii) In verification experiment of position and speed estimation signals, the estimated position and speed of the rotor are approximately equal to the actual value obtained by the photoelectric encoder, which proves that the speed and position information estimated by the MRAS method adopted in this paper has high accuracy.

(iii) Finally, the system closed-loop experiment shows that the designed control platform can control PMSM to follow the reference speed well under the four different working conditions: no-load reference speed of 500rpm, constant load reference speed of 300rpm, increased load reference speed of 300rpm and time-varying load reference speed of 300rpm, which proves that the hardware and software of the designed platform have high control precision degree and following ability.

ACKNOWLEDGEMENTS

The work described in this paper was supported in part by Educational Research Project for Young and Middle-aged Teachers of Fujian Provincial Department of Education (Grant No. JAT200465); the Open Fund Project of Fujian Provincial Education Department Key Laboratory of Advanced Motion Control (Minjing University) (Grant No. MU-AMC202103); the Science and Technology Planning Project of Xiamen (Grant No. 3502Z0203066).

REFERENCES

[1] LI Ye, YAN Xin-pin (2001) The perspective and status of PMSM electrical servo system. Micromotors 4:30-33
[2] WANG Hua, ZOU Ji-hao (2004) Direct thrust control of permanent magnet linear synchronous motor based on fuzzy logic. Chinese Journal of Electron Devices 6:2280-2283
[3] WANG Hong, YU Yong and XU Dian-guo (2007) The position servo system of PMSM. Proceedings of CSEE 7:151-155
[4] Tarczewski T., Niewiara L. J. and Grzesiak L. M. (2020) Artificial bee colony based state feedback position controller for PMSM servo-drive - The efficiency analysis. Bulletin of the Polish Academy of Sciences: Technical Sciences 4:997-1007
[5] Khelouat Lila, Ahriche Aimad and Mekhilef Saad (2021) State feedback control of stabilization of PMSM-based servo-drive with parametric uncertainty using interval analysis. International Transactions on Electrical Energy Systems 11:1-4
[6] Yeam Tae-il, Lee Dong-Choon (2021) Design of sliding-mode speed controller with damping control for single-inverter dual-PMSM drive systems. IEEE Transactions on Power Electronics 5:5794-5801
[7] B. Singh, B.P. Singh, S. Dwivedi (2009) A review of sensor reduction techniques in permanent magnet synchronous motor drives. International Jornal of Power and Energy Systems 1:10–18
[8] F. Genduso, R. Miceli, C. Rando, G.R. Galluzzo (2010) Back EMF sensorless-control algorithm for

Forest Chemicals Review
www.forestchemicalsreview.com
ISSN: 1520-0191
September-October 2021 Page No. 1091-1118
Article History: Received: 22 July 2021 Revised: 16 August 2021 Accepted: 05 September 2021 Publication: 31 October 2021

high-dynamic performance PMSM. IEEE Transactions on Industrial Electronics 6:2092–2100
[9] Y.H. Kim, Y.S. Kook (1999) High performance IPMSM drives without rotational position sensors using reduced-order EKF. IEEE Transactions on Energy Conversion 4:868-873
[10] S. Bolognani, M. Zigliotto, M. Zordan (2001) Extended-range PMSM sensorless speed drive based on stochastic filtering, IEEE Transactions on Power Electronics 1:110-117
[11] B.B.Akin (2004) Acomparative study on non-linear state estimators applied to sensorless AC drives: MRAS and Kalman filter. Proceedings of Industrial Electronics Society conference: 2148-2153
[12] M. Boussak (2005) Implementation and experimental investigation of sensorless speed control with initial rotor position estimation for interior permanent magnet synchronous motor drive. IEEE Transactions on Power Electronics 6:1413-1421
[13] M.S. Islam, I. Husain, R.J. Veillette, C. Batur (2003) Design and performance analysis of sliding-mode observers for sensorless operation of switched reluctancemotors. IEEE Transactions on Control Systems Technology 3:383-389
[14] L. Jiaxi, Y. Guijie, L. Tiecai (2007) A new approach to estimated rotor position for PMSM based on sliding mode observer. Proceedings of International on Electrical Machines and Systems Conference: 426–431
[15] N. Bianchi, S. Bolognani, J. Jang, S. Sul (2007) Comparison of PM motor structures and sensorless control techniques for zero-speed rotor position detection. IEEE Transactions on Power Electronics 6:2466–2475
[16] J. Hu, J. Liu, L.X. Eddy (2008) Current effects on rotor position estimation and magnetic pole identification of PMSM at zero and low speeds. IEEE Transactions on Power Electronics 5:2565-2575
[17] D. Raca, P. García, D.D. Reigosa, F. Briz, R.D. Lorenz (2010) Carrier-signal selection for sensorless control of PM synchronous machines at zero and very low speeds, IEEE Transactions on Industrial Applications 1:167–178
[18] A. Yoo, K.S. Sul (2009) Design of flux observer robust to interior permanent-magnet synchronous motor flux variation, IEEE Transactions on Industrial Applications 5:1670-1677
[19] S. Maiti, C. Chakraborty, S. Sengupta (2009) Simulation studies on model reference adaptive controller based speed estimation technique for the vector controlled permanent magnet synchronous motor drive, Simulation Modelling Practice and Theory 4:585-596
[20] Y.S. Kim, Y.K. Choi, J.H. Lee (2005) Speed sensorless vector control for PMSM based on instantaneous reactive power in the wide speed range, Electric Power Applications IEE Proceedings 5:1343–1349
[21] Q. An, L. Sun (2008) On-line parameter identification for vector controlled PMSM drives using adaptive algorithm, in: Proceedings of Vehicle Power and Propulsion Conference: 1-6
[22] M. Rashed, P.F.A. Mac Connell, A.F. Stronach, P. Acarnley (2007) Sensorless indirect rotor-field-orientation speed control of a permanent-magnet synchronous motor with stator-resistance estimation. IEEE Transactions on Industrial Electronics 3:1664-1675
[23] W. Zhifu, T. Qizhi, Z. Chengning (2009) Speed identification about PMSM with MRAS, in: Proceedings of Power Electronics and Motion Control conference: 1880-1884
[24] Fayez F. M. El-Sousy, Khaled A. Abuhasel (2014) Adaptive recurrent functional-link-based petri fuzzy-neuralnetwork controller for a DSP-based Induction motor servo drive system. WSEAS Transactions on Circuits and Systems 13:381-404
[25] A. Khlaief, M. Boussaka, A. Châari (2014) A MRAS-based stator resistance and speed estimation for sensorless vector controlled IPMSM drive. Electric Power Systems Research 108:1-15

Forest Chemicals Review
www.forestchemicalsreview.com
ISSN: 1520-0191
September-October 2021 Page No. 1091-1118
Article History: Received: 22 July 2021 Revised: 16 August 2021 Accepted: 05 September 2021 Publication: 31 October 2021

[26] Fayez F. M. El-Sousy, Khaled A. Abuhasel (2019) Intelligent adaptive dynamic surface control system with recurrent wavelet elman neural networks for DSP-based Induction motor servo drives. IEEE Transactions on Industry Applications 2:1998-2020

[27] L.F. Cui, X.Y. Xue, S.M. Ding and F.X. Le (2019) Development of a DSP-based electronic control system for the active spray boom suspension. Computers and Electronics in Agriculture 166:1-9

[28] Wei-Lun Huang, Yen-Han Wang, Fu-Chung Kuo, et al. (2021) Integrating time-optimal motion profiles with position control for a high-speed permanent magnet linear synchronous motor planar motion stage. Precision Engineering 68:106-123

[29] Wen-Chun Chi, Ming-Yang Cheng (2014) Implementation of a sliding-mode-based position sensorless drive for high-speed micro permanent-magnet synchronous motors. ISA Transactions 53:444-453

[30] Mitsubishi Eletric (2003) Data Sheet of PM50RLA60.

[31] WANG Shao-zhu, HUANG Tao (2012) Direct torque control of permanent magnet synchronous motor based on expected voltage vector. Electric Machines and Control Application 2:25-30

[32] LIN Rui-quan, HUANG Tao and ZHANG Tao (2012) A composite speed estimation algorithm of PMSM. Journal of Harbin University of Science and Technology 4:1-7

[33] XIAO Chun-yan. Research and realization of SVPWM. Graduate degree in engineering. Nanchang University, China, 2005.